CHAPTER 13

Molecular Motors: Examples

Alex Mogilner, Tim Elston, Hongyun Wang and George Oster

13.1 Switching in the bacterial flagellar motor

As an example of the numerical algorithm developed in the previous chapter, we consider a model for switching in the bacterial flagellar motor proposed by Scharf et al. [Scharf et al., 1998]. Some bacteria, such as *Escherichia coli*, swim by spinning long helical flagella. Each cell has multiple flagella, all of which have the same handedness. When the flagella are spun in the counterclockwise (CCW) direction, they come together to from a bundle that propels the cell through the fluid. The motor that is responsible for flagella rotation is reversible. When spun in the clockwise (CW) direction, the flagella fly apart and the cell undergoes a tumbling motion. Addition of a chemical attractant causes the cell to suppress tumbling when moving toward the food source. One of the proteins in the signaling pathway is CheY. The binding of phosphorylated CheY to the portion of the motor located within the cytoplasm promotes CW rotation. To model motor reversals, the protein complex which forms the rotor is assumed to exist in two distinct conformational states that correspond to CW and CCW rotation. The binding of CheY decreases the free energy of the CW state, while at the same time increasing the free energy of the CCW by an equivalent amount. To capture this effect, the free energy of the rotor is assumed to have the following form (see Fig. 13.1A):

$$G(x) = 4\Delta G_{nb}\left(\frac{x^4}{4} - \frac{x^2}{2}\right) - \frac{1}{2}\Delta G x, \tag{13.1}$$

where x is an appropriate reaction coordinate and $\Delta G = G(-1) - G(1)$ is the free energy difference between the CW and CCW states. $\Delta G_{nb} = G(0) - G(-1)$ is the free energy difference between the transition state and either the CW or CCW state when

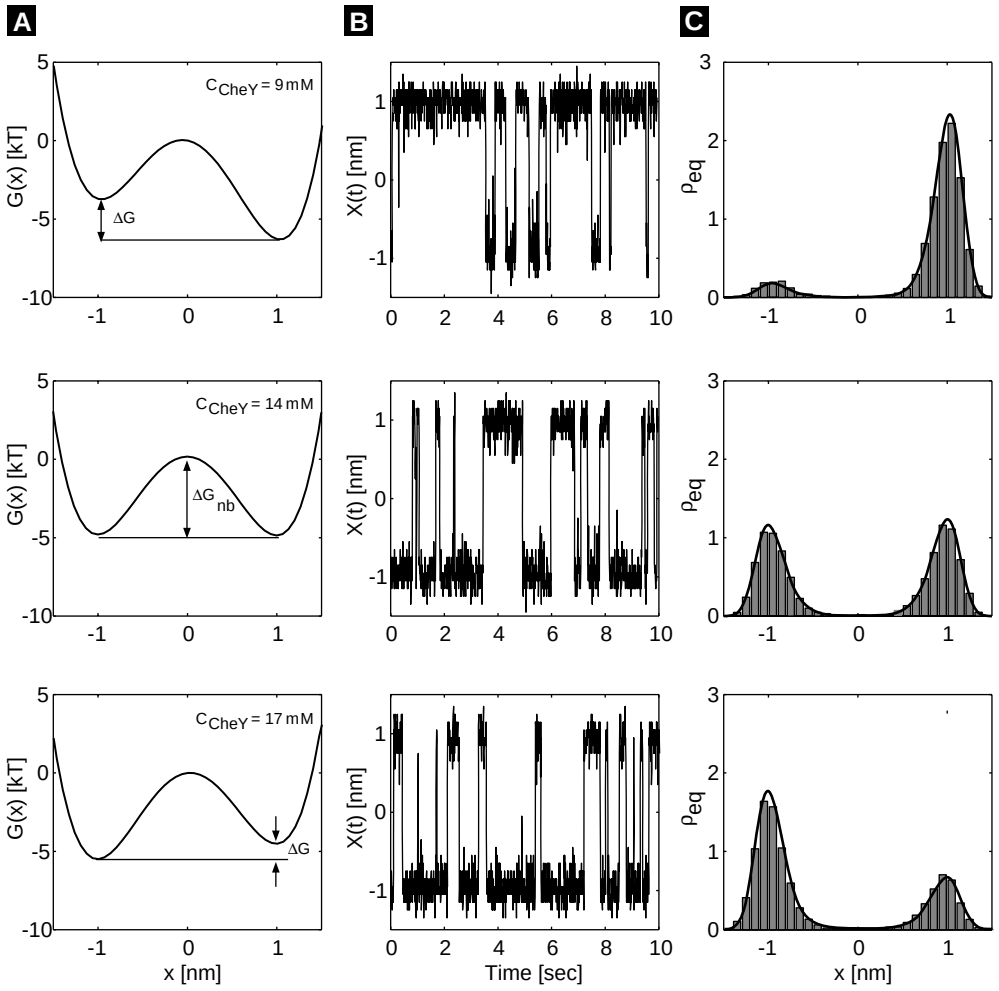

Figure 13.1 (A) The free energy digram for the rotor at various levels of CheY concentration. (B) Time series generated from the three potentials shown in A. (C) The stationary distributions for the three potentials shown in A.

the CheY concentration is such that $\Delta G = 0$ (i.e., there is no bias toward CCW or CW rotation).

To model the chemical kinetics of CheY, we assume that the binding of CheY to the motor is a two state processes with a single binding site either being empty or occupied. Let $p_E(t)$ be the probability that the site is empty at time t and $p_O(t)$ be the probability that the site is occupied. The probabilities satisfy the following set of coupled equations:

$$\frac{dp_E(t)}{dt} = -k_{on}p_E(t) + k_{off}p_O(t), \tag{13.2}$$

$$\frac{dp_O(t)}{dt} = -k_{off}p_O(t) + k_{on}p_E(t), \tag{13.3}$$

where k_{off} is the dissociation rate constant and k_{on} is the rate at which CheY binds to the motor. From the law of mass action, k_{on} should be proportional to the CheY concentration. That is, $k_{on} = k'_{on}[\text{CheY}]$, where k'_{on} is a second order rate constant and the brackets stand for concentration. If the concentration of CheY is held constant, then p_E and p_O will relax to their equilibrium values. These are found by solving (13.2) and (13.3) with the time derivatives set equal to zero. Doing this yields $p_O = [\text{CheY}]/(\text{K}_\text{d} + [\text{CheY}])$ where $K_d = k_{off}/k'_{on} = 9.1$ μM is the dissociation constant.

There are approximately 26 binding sites on the motor, and the average number of occupied sites is $26p_O$. In the absence of CheY, $\Delta G = \Delta G_0 = 14k_BT$ and at saturating concentrations of CheY, $\Delta G = \Delta G_\infty = -9k_BT$. Therefore, the change in ΔG from low to high CheY concentrations is $\Delta\Delta G = \Delta G_0 - \Delta G_\infty = 23k_BT$, where the symbol $\Delta\Delta G$ indicates that we are talking about a change in the value of ΔG. Thus each CheY contributes roughly $.88k_BT$ towards changing the relative free energy of the CW and CCW states. These considerations lead to the following expression for ΔG:

$$\Delta G = \Delta G_0 - \Delta\Delta G\frac{[\text{CheY}]}{\text{K}_\text{d} + [\text{CheY}]} \tag{13.4}$$

Graphs of the free energy at various CheY concentrations are shown in Fig. 13.1A, with two minima located roughly at $x = \pm 1$ Generally, we shall measure distance, x, in nanometers (nm) and force in picoNewtons (pN). In these units $k_BT = 4.1$ pN-nm at room temperature (T = 298 K). The force that arises from changes in free energy is $-\partial G/\partial x$. Therefore, the force vanishes at the minima. Additionally, if the conformation of the rotor is slightly displaced from either minima, it experiences a force that moves it back towards that minimum. The force also vanishes at the local maximum located near $x = 0$. However, when the conformation of the rotor is slightly displaced from the origin, the force acts to move away from the rotor at $x = 0$ and toward one of the two minima. Thus, we expect the rotor to spend most of its time near the minima. To surmount the energy barrier between the minima requires a substantial thermal fluctuation.

The reaction coordinate $x(t)$, which determines the state of the rotor, can take on values anywhere between $\pm\infty$. Clearly we cannot use an infinite interval in our numerical algorithm. However, since $G(x) \to \infty$ as $x \to \pm\infty$, there is a strong restoring force that drives the reaction coordinate back toward the origin when $|x|$ is large. This means that the probability of finding $x(t)$ at distances far from the origin is small and ignoring large values of $|x|$ will not significantly affect our numerical solutions. For the parameters we shall consider, the interval $(-2, 2)$ is wide enough to ensure numerical accuracy. In practice, an appropriate interval can be determined by successively enlarging the length until the numerical results no longer change appreciably. At $x = \pm 2$, we enforce reflecting boundary conditions as described in Section 12.5.2. The diffusion

equation for this process is:

$$\frac{\partial p}{\partial t} = D\frac{\partial}{\partial x}\left(\frac{\partial G(x)}{\partial x}\frac{p}{k_B T} + \frac{\partial p}{\partial x}\right). \tag{13.5}$$

To find the equilibrium distribution for $p(x,t)$, the above equation is solved with $\partial p/\partial t = 0$. This yields:

$$p_{eq}(x) = \frac{\exp\left(-\frac{G(x)}{k_B T}\right)}{\int_{-\infty}^{\infty}\exp\left(-\frac{G(y)}{k_B T}\right)dy}. \tag{13.6}$$

The diffusion coefficient D in (13.5) represents an effective diffusion coefficient for the reaction coordinate that includes many microscopic effects. For all the results presented below $D = 70$ nm^2/sec and $\Delta G_{nb} = 5k_B T$. These values were chosen to be consistent with experimental observation that at 14 μM of CheY, motor reversals occur at an average rate of 2 sec^{-1} (we expand on this point below). Fig. 13.1B shows time series generated by the three potentials shown in Fig. 13.1A. The bistable nature of the system is clearly evident. The time series can be used to produce histograms of the reaction coordinate. An approximation for $p_n^{(s)}$ is constructed by dividing the number of points in each bin of the histogram by the total number of points in the time series. Then we estimate $p(x_n) \approx p_n^{(s)}/\Delta x$. Fig. 13.1C shows distributions generated in this fashion.

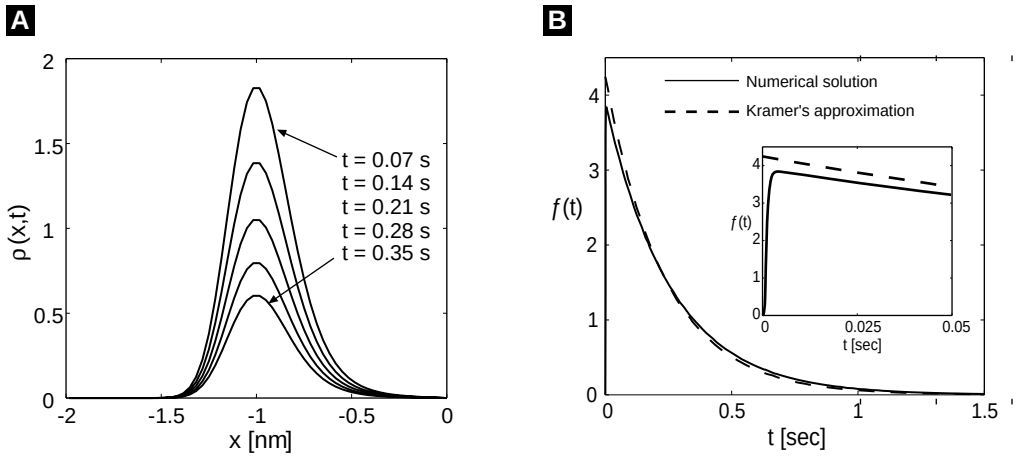

Figure 13.2 Numerical results of the first passage time problem. The concentration of CheY has been chosen such that $\Delta G = 0$. At $t = 0$, the reaction coordinate is placed at $x = -1$. An absorbing boundary is placed at $x = 0$ and a reflecting barrier at $x = -2$. The first passage time is the time for the reaction coordinate to reach the origin. (A) Time evolution of the probability density. As time increases, the probability that the reaction coordinate remains inside the region decreases. (B) Probability density of the first passage time. Inset: an expanded view of the probability density near the origin showing the nonexponential nature of the distribution.

The solid lines are the exact results given by (13.6). As is clearly seen from the figure, the numerical algorithm accurately reproduces the equilibrium distribution.

In the discussion of Markov chains and diffusion in the previous chapter, we encountered the idea of a waiting or first passage time. This is a very important mathematical concept that comes up in many different biological contexts. At a CheY concentration of 14 μM the motor reverses roughly twice per second and there is no bias toward CW or CCW rotation. To compute the switching rate, we must compute the average time for the system located at the reaction coordinate x to surmount the energy barrier at $x = 0$. To this end, the reaction coordinate is started at $x = -1$ at $t = 0$ with an absorbing boundary at $x = 0$. Fig. 13.2A shows the numerically generated probability density at various times. To generate this figure, 61 grid points were used. Note that the probability of finding the particle in the interval $(-\infty, 0)$ is continuously decreasing, due to the absorbing boundary. This probability can be used to determine the first passage time density $f(t)$ through the relation:

$$f(t) = -\frac{d}{dt}\text{Prob}\left[-\infty < x(t) < 0\right] = -\frac{d}{dt}\int_{-\infty}^{0} p(x,t)dx \approx$$
$$-\frac{d}{dt}\sum_{n=1}^{M} p_n(t) = p_M F^{abs}_{M+1/2}, \tag{13.7}$$

where the last equality follows from (12.42) and the absorbing boundary condition. Therefore, the numerical algorithm is well suited for computing first passage time densities. Fig. 13.2B shows the first passage time density. The solid line is the numerical result. The dashed line is Kramer's approximation, which assumes the process has an exponential distribution with mean first passage time

$$\text{MFPT} \approx \frac{k_B T \pi}{D\sqrt{G''(-1)|G''(0)|}} \exp\left(\frac{G(0) - G(-1)}{k_B T}\right)$$
$$= \frac{k_B T \pi}{D\sqrt{32}\Delta G_{nb}} \exp\left(\frac{\Delta G_{nb}}{k_B T}\right). \tag{13.8}$$

A derivation of this result can be found in [Gardiner, 1997]. Note that the most significant factor in determining the mean first passage time is ΔG_{nb}. The validity of Kramer's approximation depends on $\Delta G_{nb} >> k_B T$. As shown in the inset of Fig. 13.2B, the first passage time distribution is not exponentially distributed, since it must be equal to zero at $t = 0$. However, if we ignore this very short initial time interval, the distribution is approximated reasonably well with an exponential. Using the numerical distribution to compute the mean first passage time, we find MFPT$= = 0.253$ sec, and using Kramer's approximation (13.8) we find MFPT$= 0.236$ sec. An exact expression [Gardiner, 1997] gives MFPT$= 0.259$ sec. The agreement between this value and the numerical result given above provides evidence that the algorithm is faithfully reproducing the dynamics of the system. The switching rate is $1/(2MFPT) = 1.98$ sec^{-1}, where the factor of $1/2$ comes from the fact that half the time the reaction coordinate surmounts the barrier it falls back into well from which it started. This justifies our choice of D and ΔG_{nb}.

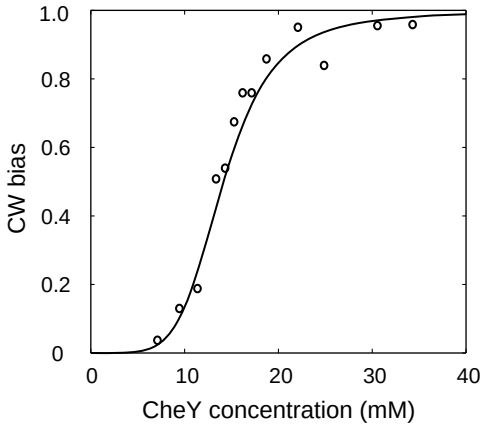

Figure 13.3 The CW bias as function of CheY concentration. The solid line is the model prediction and the data points are from Scharf et al. [Scharf et al., 1998]

To test this simple model, we compute the CW bias as a function of CheY concentration. The CW bias is the fraction of time that the motor spends rotating in the CW direction. This can be computed by integrating (13.6) over the interval $(-\infty, 0)$. That is,

$$\text{CW bias} = \frac{\int_{-\infty}^{0} \exp\left(-\frac{G(x)}{k_B T}\right) dx}{\int_{-\infty}^{\infty} \exp\left(-\frac{G(y)}{k_B T}\right) dy}. \tag{13.9}$$

Fig. 13.3 shows a comparison of the model's predictions to the experimental data of Scharf et al [Scharf et al., 1998]. The agreement between the data and the theoretical curve provides evidence to support the model's validity.

13.2 A motor driven by a "flashing potential"

The following process called the *flashing ratchet* [Doering, 1995, Doering, 1998] is a paradigm for molecular motors. It is also a good application for the methods developed in the previous chapter. Imagine a protein driven by alternating its exposure to two potential energy profiles: V_1 (solid line) and V_2 (dashed line), as shown in Fig. 13.4. The first potential is a piecewise linear asymmetric sawtooth potential, while the second potential is a constant. Thus, in the first potential, the protein is localized near a local minimum, while in the second potential the protein diffuses freely. While in either potential, the motion of the particle is given simply by $\zeta dx/dt = -dV_i/dx + f_B(t), i = 1, 2$. Switching between the potentials is governed by a chemical reaction (vertical arrows), which occurs with the rate k.

Clearly, if the sawtooth potential is symmetric, the average displacement of the protein must be zero. However, in the case of the asymmetric potential shown in Fig. 13.4, the protein on the average moves to the right, although all steps are reversible.

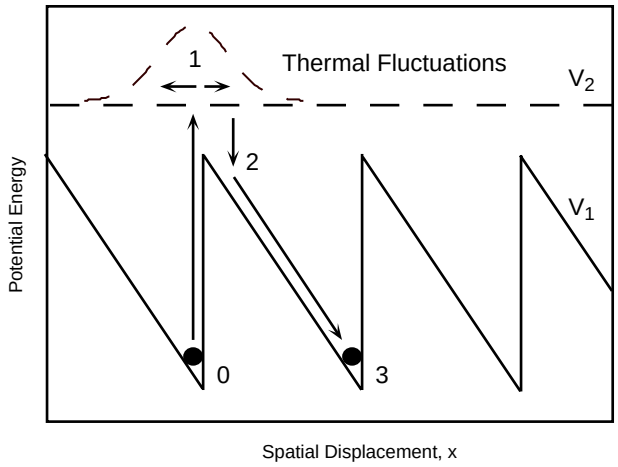

Figure 13.4 The flashing ratchet. In the first potential, the protein is localized near a local minimum. Alternatively, the protein is free to diffuse. When the first potential is switched back on, the protein settles into the nearest local minimum.

This phenomenon can be easily understood, when the following inequalities are valid:

$$\frac{k_B T L}{FD} \ll \frac{1}{k} \ll \frac{L^2}{D}. \tag{13.10}$$

Here L is the wavelength of the sawtooth potential, and $F = -dV_1/dx$ is the slope of the first potential, i.e. the force driving the protein to the right in the first potential. The corresponding drift rate of the protein is $F/\zeta = FD/k_B T$. The order of magnitude of the time for the protein to drift into a local minimum is $k_B TL/FD$. The diffusion in the first potential and the protein's deviations from a local minimum can be neglected if the slope of the sawtooth potential is very steep. Quantitatively, this means that $k_B T \ll FL$ (or $k_B TL \ll FL^2$ (compare with (13.10)).

The first inequality (13.10)) means that the protein reaches a local minimum of the sawtooth potential well before this potential switches off. The second inequality (13.10) indicates that when the protein diffuses freely, it rarely can move farther than distance L, before the sawtooth potential is switched back on: the mean time between "flashes" of the potential, $1/k$, is much less, than the characteristic diffusion time L^2/D. Thus by the time the sawtooth potential is switched off, the protein is in a local minimum. When the sawtooth potential is switched off, the protein diffuses with equal probability to the left and to the right, and will not diffuse very far compared to the period of the potential. If the protein diffuses to the left, then by the time the sawtooth potential is switched back on, the protein is in the *basin of attraction* of the same local minimum it started from. When the potential is on, the protein returns to the starting point of the cycle. However, if the diffusion to the right took place, the protein is in the basin of attraction of the next local minimum to the right. Thus, the protein either does not move, or moves the distance L to the right, with equal probability. Said another way, the diffusion in the flat potential can be viewed as a spreading Gaussian distribution. The asymmetry of the sawtooth potential, when it is switched on, cuts a larger portion of the distribution into the next domain of attraction. The corresponding average rate

of motion is $\langle V \rangle = Lk/4$ (the mean duration of a cycle is $2/k$ and, on average, the system steps a distance L per two cycles).

We considered the highly peculiar sawtooth potential with one of the slope being infinitely steep. For more regular, smooth potentials, the velocity of the flashing ratchet is computed analytically in the so called "fast" and "slow flashing" limits [Doering, 1995]. In both of these limits, the protein advances very slowly. If the flashing is too fast, the protein does not have time to reach the local minimum, and the effect of asymmetry is lost. The protein is effectively exposed to the average potential which does not support any steady movement. On the other hand, if the flashing is too slow, the freely diffusing protein moves too far from a local minimum, the information about its initial position is lost, and the average displacement becomes very small. The mean velocity of the flashing ratchet reaches maximum $\sim Lk/4$ (for the smooth asymmetric potential, such that $\delta V \sim k_B T$), when $k \sim D/L^2$ (flashing frequency is of the same order of magnitude as the inverse time to diffuse over the potential's period).

In the general case, the average velocity of the flashing ratchet can be computed only numerically. Following the methods of the previous chapter, we can describe the ratchet by two coupled Smoluchowsky equations:

$$\frac{\partial p_i}{\partial t} = D\frac{\partial}{\partial x}[\frac{\partial p_i}{\partial x} + \frac{\partial V_i/\partial x}{k_B T}p_i] + k(-p_i + p_j), \quad i = 1, 2, \ j \neq i. \tag{13.11}$$

These equations must be solved numerically (see Exercise 2) on the finite domain $[0, L]$ with periodic boundary conditions and normalization condition:

$$\int_0^L (p_1(x, t = 0) + p_2(x, t = 0))dx = 1.$$

When the probability distributions achieve steady state, the net current is

$$J = -D[\frac{\partial^2(p_1 + p_2)}{\partial x^2} + \frac{\partial V_1/\partial x}{k_B T}p_1],$$

from which the average velocity can be found: $\langle V \rangle = LJ$.

It is important to realize that in the process energy is consumed from the chemical reaction that drives the switching between the two potentials. The motion down the slope of the sawtooth potential $2 \to 3$, generates heat by frictional dissipation. Finally, if a small load force directed to the left is applied to the protein, the movement slows down. The load force is equivalent to tilting the potential to the left. Thus, the flashing ratchet is able to generate force, and has all characteristics of a molecular motor. However, there is no direct correspondence of the flashing ratchet mechanism to a real motor. In what follows, we consider two simple models of actual molecular motors.

13.3 The polymerization ratchet

Perhaps the simplest way to convert chemical energy into a mechanical force is by polymerizing a filament against a load force (see the previous chapter). Here the energy

source is the free energy of binding of a monomer onto the tip of the polymer, ΔG_b. If a polymer assembles against no resistance, the polymerization velocity (elongation rate) is simply

$$V_p = L(k_{on}M - k_{off}), \tag{13.12}$$

where L [nm] is the size of the monomer, M [μM] the monomer concentration, and k_{on} [(μM·sec)$^{-1}$], k_{off} [sec^{-1}] are the polymerization and depolymerization rate constants, respectively.

If an object is placed ahead of the growing polymer there are two mechanisms by which the polymer can "push" the object: (i) by rectifying the Brownian motion of the object, (ii) by actively "pushing" against the object, i.e. a power stroke. First, we discuss the Brownian ratchet. We assume that the polymer is anchored at the left end and is perfectly rigid. The object has a diffusion coefficient, $D = k_BT/\zeta$. For the moment, we neglect depolymerization ($k_{off} = 0$). In order for a monomer to bind to the end of the filament the object must open up a gap of size L by diffusing away from the tip, and remaining there for a time $\sim (k_{on}M)^{-1}$ to allow a polymerization event to take place. In the limiting case when polymerization is much faster than diffusion, i.e. $k_{on}M \gg D/L^2$, we can consider the polymerization to happen instantaneously once a gap of size L appears. Then the time for the load to diffuse a distance L is simply the mean first passage time $\langle T\rangle = L^2/2D$. To cover N such intervals takes $N\cdot\tau$ time units, so the average velocity is simply $\langle V_p\rangle = NL/(N\cdot\langle T\rangle) = 2D/L$. This is the speed of an ideal Brownian ratchet. Note that by reducing the size of the monomer, L, the speed of the ratchet increases since the likelihood of a thermal fluctuation of size L increases exponentially as L decreases. However, this is true only as long as our approximation holds: $k_{on}M \gg D/L^2$, or $L \gg \sqrt{D/(k_{on}M)}$. For smaller values of L the polymerization reaction becomes the limiting factor, so that $V_p \simeq L\cdot k_{on}M$ (c.f. (13.12) with $k_{off} = 0$).

We can picture the situation as shown in Fig. 13.5B: the object diffuses on a "staircase" sequence of identical free energy functions, $\phi(x)$, each with a step height of the monomer binding free energy, $\Delta G = -k_BT\ln(k_{on}M/k_{off})$. If a load force, F_L, opposes the diffusive motion of the object, the potential becomes $\phi(x) - F_Lx$. This corresponds to tilting the potential so that the object must diffuse "uphill", as shown in Fig. 13.5B.

Including the depolymerization rate complicates the analysis considerably. However, a diffusion equation can be formulated that can be solved exactly when $k_{on}ML, k_{off}L \ll 2D/L$. In this regime, the approximate load-velocity relationship is given by the simple formula [Peskin et al., 1993]:

$$V_p = L(k_{on}Me^{-f_LL/k_BT} - k_{off}). \tag{13.13}$$

That is, the polymerization rate in (13.13) is weighted by a Boltzmann factor where the exponent, F_LL/k_BT is the work done by the load in moving the object one step distance, L. The stall load, F_s, is reached when the work done in moving the object a distance L is just equal to the free energy from the binding reaction, so that $V_p = 0$:

$$F_s = \frac{k_BT}{L}\ln[\frac{k_{on}M}{k_{off}}]. \tag{13.14}$$

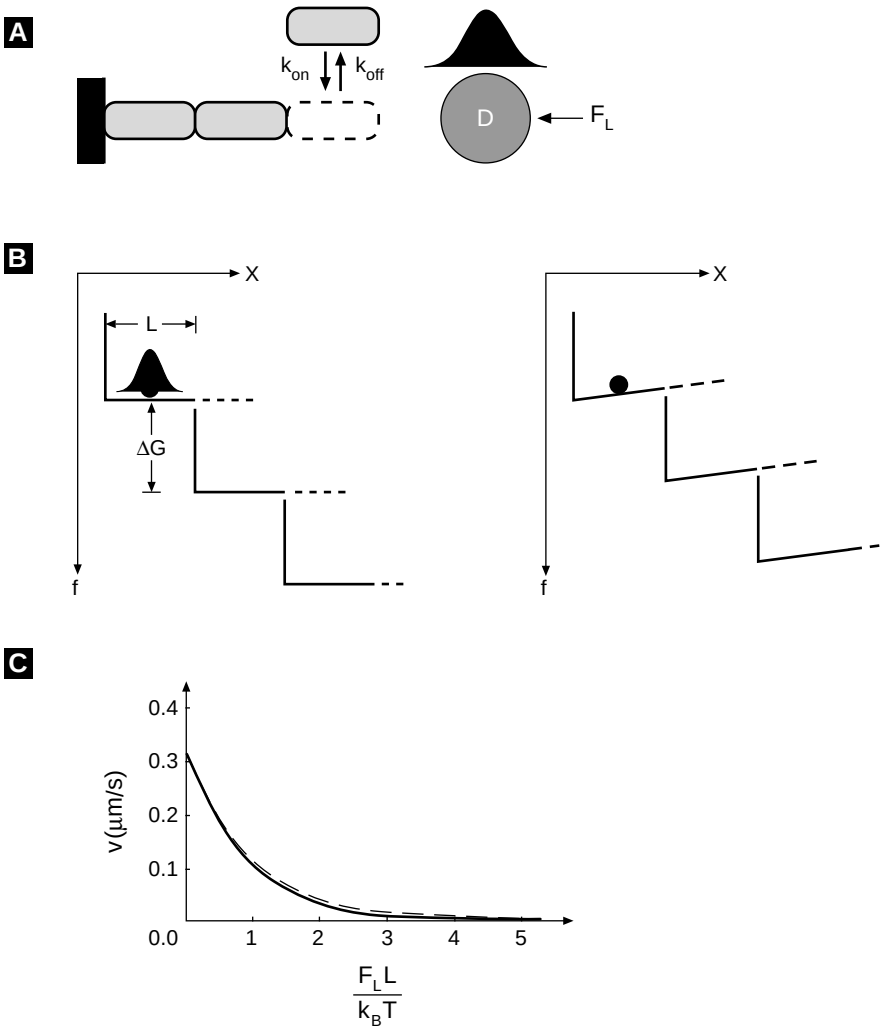

Figure 13.5 The polymerization ratchet. (a) Monomers of length L polymerize onto the end of a growing filament with rate constants k_{on}, k_{off}. An object with diffusion coefficient D has its thermal motions rectified by the insertion of each new monomer. A load force, F_L, opposes the the motion of the object to the right. (b) Free energy diagram of the polymerization process. The total free energy $\Delta G = \Delta G_b + F_L x$ where the binding free energy, $\Delta G_b \gg k_B T$. Left panel: $F_L = 0$, right panel: $F_L > 0$ tilts the potential so that the object must diffuse uphill. (c) The load-velocity curve for the polymerization ratchet given by the approximate (13.13). The exact solution is shown by the dashed line [Peskin et al., 1993].

Note that without depolymerization, $k_{off} \to 0$, there is no finite stall load.

Variations and elaborations on the polymerization ratchet have been used to model a variety of cellular processes, including lamellipodial protrusion [Mogilner and Oster, 1996], the polymerization of microtubules [Mogilner and Oster, 1999], the propulsion of in-

tracellular pathogens [Mogilner and Oster, 1996] and the translocation of proteins [Simon et al., 1992, Peskin et al., 1993].

13.4 Model of a simple molecular motor

To illustrate the formalism developed in the previous chapter, we shall examine in detail a simplified model based on the principle of the ion-driven F_o motor of ATP synthase [Elston et al., 1998, Dimroth et al., 1999]. This enzyme uses electrochemical energy stored in a proton motive force across the inner membrane of mitochondria to produce ATP. This will illustrate many of the principles of mechanochemical energy conversion by proteins, but is sufficiently simple to analyze analytically and numerically. The motor is sketched schematically in Fig. 13.6. It consists of two reservoirs separated by an ion impermeable membrane. The reservoir on the left is acidic (high proton concentration) with concentration c^{acid}, and the reservoir on the right is basic (low concentration) with concentration c^{base}. The motor itself consists of two "parts:" (i) a "rotor" carrying negatively charged sites spaced a distance L apart that can be protonated and deprotonated; (ii) a "stator" consisting of a hydrophobic barrier that is penetrated by an apolar strip that can allow a protonated site to pass through the membrane, but will block the passage of an unprotonated site. (The height of the energy barrier blocking passage of a charge between two media with different dielectric constants ϵ_1 and ϵ_2 is $\Delta G \simeq 200[(1/\epsilon_1) - (1/\epsilon_2)] \simeq 45 k_B T$ [Israelachvili, 1992, Dimroth et al., 1999]. This energy penalty arises from the necessity of stripping hydrogen bonded water molecules from the rotor sites.)

Qualitatively, the motor works like this. Rotor sites on the acidic side of the membrane are frequently protonated. In this state (a nearly neutral dipole) the rotor can diffuse to the right allowing the protonated site to pass through the membrane-stator interface to the basic reservoir. Once exposed to the low proton concentration in the basic reservoir, the proton quickly dissociates from the rotor site. In its charged state, the rotor site cannot diffuse backwards across the interface: its diffusion is "ratcheted." We will show that thermal fluctuations will consistently drive the rotor to the right in Fig. 13.6.

Thus a rotor site can exist in two states: unprotonated and protonated. To specify the mobility state of the rotor, we need to keep track only of the site immediately adjacent to the membrane on the acidic side. In its unprotonated state, the site adjacent to the membrane is immobilized since it cannot pass into the stator, nor can it diffuse to the left since the next rotor site on the basic side of the membrane is almost always deprotonated, and cannot diffuse to the left. (Of course, this depends on the thickness of the membrane being the same as the rotor spacing; this is unrealistic, but the full model treated in the references does not have this constraint.) Thus the progress of the model can be pictured as a sequence of transitions between two potentials, as shown in Fig. 13.6. When deprotonated, the rotor is immobilized in potential ϕ_d, and when protonated, it can move in potential ϕ_p. The effect of the load force, F_L, is to tilt the

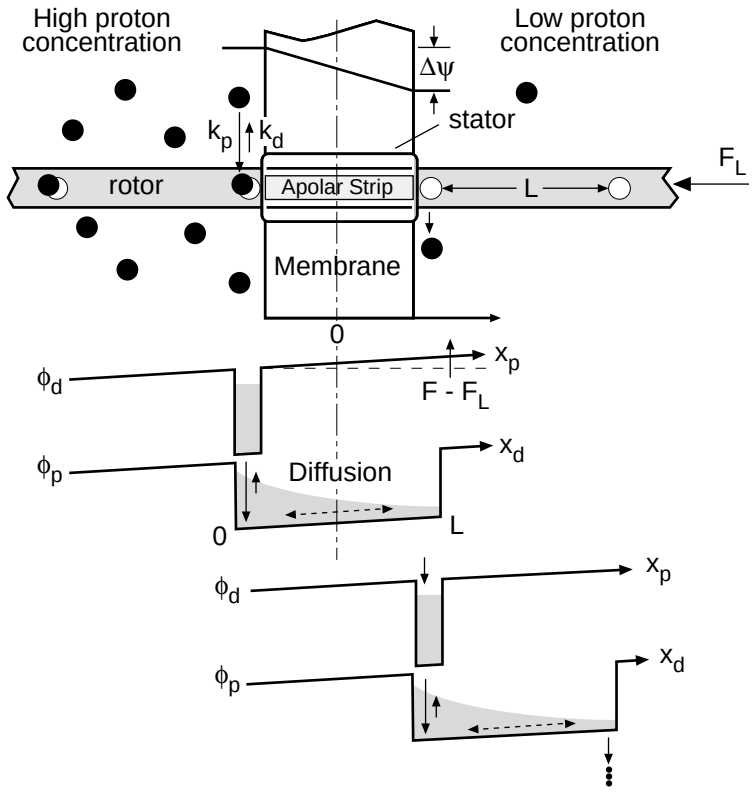

Figure 13.6 Simplified model illustrating the principle of the F_o motor. The state of the rotor can be pictured as a probability cloud (shown shaded) that drains from one potential to the next. ϕ_p is the potential seen by the site adjacent to the left side of the membrane in the protonated state, and ϕ_d is the potential in the deprotonated state. The potentials are tilted by an amout equal to the difference between the driving force ($F_I = e \cdot d\psi/dx$), and the load force, F_L. In the deprotonated state the site is immobilized, and in the protonated (almost neutral) state it can diffuse in the potential well ϕ_p. In the fast diffusion limit, the probability cloud quickly settles into the exponential Boltzmann distribution inside ϕ_p, which determines the probability of draining into the next deprotonated well, thus completing one step to the right.

potentials upward, so the motion in potential ϕ_p is "uphill" (i.e. the total potential when protonated can be written as $\phi_p(x) - F_L x$).

Below, we consider two limiting cases. In the first one, diffusion is much faster than the chemical reaction rates. In the second one, the diffusion time scale is comparable to the reaction rates in the basic reservoir. The first case can be treated *analytically*, while the second one will require *numerical* simulation.

13.4.1 The average velocity of the motor in the limit of fast diffusion

The model can be formulated mathematically in terms of the probability of the deprotonated state, $p_d(t)$ [non-dimensional], and the probability density of the protonated state, $p_p(x,t)$ [1/nm]. Here $x, 0 \le x \le L$, is the distance of the protonated site from the interface between the acidic reservoir and the membrane. The model equations have the form:

$$\begin{aligned}\frac{dp_d}{dt} &= \text{Net deprotonated spatial flux} + \text{Net reaction flux} \\ &= J_{x_d} + J_\xi \end{aligned} \tag{13.15}$$

$$\begin{aligned}\frac{\partial p_p}{\partial t} &= \text{Net protonated spatial flux} - \text{Net reaction flux} \\ &= J_{x_p} - J_\xi \end{aligned} \tag{13.16}$$

where

$$\begin{aligned} J_{x_d} &= 0 \\ J_{x_p} &= D\frac{\partial}{\partial x}\left(\frac{\partial p_p}{\partial x} - \frac{F_I - F_L}{k_B T}p_p\right),\ J_{x_p}(0) = J_{x_p}(L) = 0 \\ J_\xi &= \text{deprotonation at acidic reservoir} \\ &\quad + \text{deprotonation at basic reservoir} \\ &\quad - \text{net protonation at both reservoirs} \\ &= k_d p_p(0) + k_d p_p(L) - \bar{k}_p p_d \end{aligned}$$

Protonation rates are proportional to hyrogen ion concentration on either side of the membrane, and the net protonation at both reserviors is: $\bar{k}_p = k_p c^{acid} + k_p c^{base}$. Note that the rates of protonation and deprotonation have the dimensions $\bar{k}_p$ [1/sec] and k_d [nm/sec], respectively. We assume that the deprotonation rates are the same at both reservoirs.

First we nondimensionalize the model equations using the re-scaled coordinate, $(x/L) \to x$, the re-scaled time, $(k_d t/L) \to t$, and the following dimensionless parameters:

- Ratio of reaction to diffusion time scales: $\Lambda = D/k_d L$.
- Net work done in moving the rotor a distance L : $w = (F_I - F_L)L/k_B T$.
- Equilibrium constant: $\kappa = \bar{k}_p L/k_d$.

Here $F_I = e\Delta\psi/L$ is the electrical driving force, which is assumed to be constant. Substituting these variables and parameters into equations (13.15) and (13.16) gives

$$\frac{dp_d}{dt} = -\kappa p_d + p_p(0) + p_p(1), \tag{13.17}$$

$$\frac{\partial p_p}{\partial t} = \kappa p_d - p_p(0) - p_p(1) + \Lambda \frac{\partial}{\partial x}\left(\frac{\partial p_p}{\partial x} - w p_p\right), \tag{13.18}$$

where x, t are now the non-dimensional coordinate and time, respectively.

In many situations it turns out that diffusion is much faster than the chemical reaction rates: $\Lambda \gg 1$. (At $D \sim 10^7$ nm^2/sec, $L \sim 10$ nm, $k_d \sim 10^3$ nm/sec, the order of magnitude of the parameter Λ is 10^3.) This means that the time between dissociation events is much longer than the time to diffuse a distance L, so the process is limited by the speed of the reactions, not by the diffusion of the rotor. In other words, the diffusive motion of the rotor is so fast that it achieves thermodynamic equilibrium, and so its displacement can be described by a Boltzmann distribution. In this case we can express the probability distribution as $p_p(x,t) = p_p(t) \cdot P(x)$, where $p_p(t)$ is the probability of the site being in the protonated state and $P(x)$ is the *equilibrium* spatial probability density describing the rotor's position relative to the stator.

We can obtain the steady state Boltzmann distribution, $P(x)$, from (13.18). First, we divide through by Λ and take advantage of the fact that $\Lambda \gg 1$: all terms but the last are rendered negligible, so that the distribution of rotor positions in the protonated state potential well $\phi_p (0 \le x \le 1)$ in Fig. 13.6 is governed by

$$\frac{dP}{dx} - wP = 0.$$

The solution must be normalized to 1 since it represents a probability density. The result is:

$$P(x) = \left(\frac{w}{e^w - 1}\right) e^{wx}, \quad 0 \le x \le 1, \tag{13.19}$$

where the quantity in parenthesis is the normalization factor. Thus, the rates of protonation at time t are: $p_p(0,t) = p_p(t) \cdot P(0)$ and $p_p(1,t) = p_p(t) \cdot P(1)$, respectively. Substituting this into (13.17) and imposing the conservation of probability, $p_d(t) + p_p(t) = 1$, we reduce the problem to the 2-state Markov chain described by:

$$\frac{dp_d}{dt} = -\frac{dp_p}{dt} = -\kappa p_d + (P_+ + P_-) p_p, \tag{13.20}$$

where $P_+(w) = w/(1-e^{-w})$, $P_-(w) = w/(e^w - 1)$. Therefore, the stationary probabilities are obtained directly by setting the time derivatives equal to zero and solving for p_p:

$$p_d(w,\kappa) = \frac{P_+ + P_-}{\kappa + P_+ + P_-}, \qquad p_p(w,\kappa) = \frac{\kappa}{\kappa + P_+ + P_-}, \tag{13.21}$$

or, in the dimensional variables:

$$p_d(w,\kappa) = \frac{k_d P_+ + k_d P_-}{k_p (c^{acid} + c^{base}) L + k_d P_+ + k_d P_-}, \tag{13.22}$$

$$p_p(w,\kappa) = \frac{k_p (c^{acid} + c^{base}) L}{k_p (c^{acid} + c^{base}) L + k_d P_+ + k_d P_-}. \tag{13.23}$$

The average velocity of the motor can be found using the following heuristic argument. The rotor effectively moves to the right either from the protonated state,

when the proton is released to the basic reservoir with the effective rate $k_d P_+$, or from the deprotonated state, when the protonation takes place at the acidic reservoir with the effective rate $k_p c^{acid} L$. The corresponding effective rate of movement to the right is the sum of the corresponding rates weighted by the respective state probabilities: $\langle V_r \rangle = k_p c^{acid} L p_d + k_d P_+ p_p$. Similarly, the rotor effectively moves to the left either from the protonated state, when the proton is released to the acidic reservoir with the effective rate $k_d P_-$, or from the deprotonated state, when the protonation takes place at the basic reservoir with the effective rate $k_p c^{base} L$. The corresponding effective rate of movement to the left is the sum of the corresponding rates weighted by the respective state probabilities: $\langle V_l \rangle = k_p c^{base} L p_d + k_d P_- p_p$. The net average velocity, $\langle V \rangle = \langle V_r \rangle - \langle V_l \rangle$, can be obtained by using the expressions for the state probabilities (13.22), (13.23) and some algebra:

$$\langle V \rangle (F_L) = \frac{k_p k_d L w (c^{acid} e^w - c^{base})}{(e^w - 1) k_p L (c^{acid} + c^{base}) + k_d w (e^w + 1)},$$
$$w = \frac{(F_I - F_L) L}{k_B T}. \tag{13.24}$$

As a check, note that when there is no load ($F_L = 0$), no membrane potential ($F_I = 0$), and no proton gradient ($c^{acid} = c^{base}$), the velocity vanishes, as it should. The load-velocity relationship given by (13.24) looks very similar to the one in the next limiting case, and is plotted in Fig. 13.8C.

The *stall force*, F_s, is reached when the load force just brings the motor to a halt ($c^{acid} e^w - c^{base} = 0$):

$$F_s = F_I + \frac{k_B T}{L} \ln[\frac{c^{acid}}{c^{base}}]. \tag{13.25}$$

Since the electrical driving force $F_I = e\Delta\psi / L$, (13.25) can be written as an equilibrium thermodynamic relation in terms of the energy:

$$F_s \cdot L = e\Delta\psi - 2.3 k_B T \Delta \mathrm{pH}. \tag{13.26}$$

This says that the reversible work done to move a rotor site across the membrane is equal to the work done by the electrical field plus the "entropic work" done by the Brownian ratchet. (The term "reversible" in this context means that the velocity is so slow (near stall) that we can neglect the viscous dissipation.) Dividing through by the unit charge, e, gives the work per unit charge, which is just the protonmotive force discussed previously. One point about (13.26) is worth noting. Since the motor is working against a conservative load force, as the motor approaches stall its efficiency approaches 100%. For a motor working against a viscous load, a more sophisticated treatment is required [Oster and Wang, 2000].

It may seem from (13.24) that there is a definite average velocity of the motor in the limit $T \to \infty$. In other words, the motor continues to move in the absence of thermal fluctuation. The reason is that the solution of the Lengevin and Smoluchowski equations cannot be treated as a regular perturbation problem in the limit of low

temperatures. This is a singlular perturbation problem, and the protein behavior at absolute zero temperature cannot be quantified as a simple limit of such behavior at low temperatures.

13.4.2 Brownian ratchet vs power stroke

In the last example the motion of the rotor was driven by a combination of Brownian motion and the membrane potential. The rotor diffusion is biased by the electrostatic forces that are switched off and on by the binding and dissociation of protons to the rotor sites. The membrane potential appears to drive the rotor unidirectionally without the aid of Brownian motion. However, this cannot happen without the binding and dissociation of protons, a stochastic process driven by thermally excited transitions. Thus even the "power stroke" depends on Brownian motion, so that setting $k_BT = 0$ in the model equations arrests the rotor motion. This is a fundamental distinction between molecular and macroscopic motors. The distinction between a motor driven by a "Brownian ratchet" and one driven by a "power stroke" may not be so clear in other systems.

In the polymerization ratchet model described above, the movement of the *load* is driven entirely by its Brownian motion. The chemical step simply rectifies, or biases, this motion [Peskin et al., 1993]. By comparison, the F_1 motor in ATP synthase is driven by the hydrolysis of ATP. The conformational change in the protein that constitutes the power stroke is known: binding of ATP to the catalytic site drives the change in protein shape that drives rotation. That is, the load is not driven significantly by Brownian motion; it sees the protein's conformational change as a "power stroke."

However, a closer look at how ATP binds to the catalytic site reveals that it is a multistep process involving the sequential annealing of hydrogen bonds between the protein and the nucleotide. Each step in this process is driven by Brownian motion, i.e. a thermally activated process as illustrated in Fig. 12.5. Therefore, the power stroke itself can be viewed as a kind of Brownian ratchet, one that proceeds at a smaller length scale than the protein (ATP synthase is ~ 10 nm in diameter, while the catalytic site is ~ 1 nm). Thus the distinction between a process driven by a Brownian ratchet and by a power stroke can be largely a matter of size scale; a fuzzy boundary separates the two notions. In the extreme case where the motion of the *load* is due only to its diffusion, and the role of the chemical reaction is only to inhibit diffusion in one direction, we can say the motor is a Brownian ratchet.

13.4.3 The average velocity of the motor when chemical reactions are as fast as diffusion

Next we consider a different limiting case: when the diffusion time scale is comparable to the reaction rates in the basic reservoir. In this case, we have to change the mathematical formulation of the model. We make the simplifying assumption that the proton concentration in the acidic reservoir is so high that the binding sites on that side are

always protonated. Now we define the right boundary of the membrane as the origin, and the distance between the membrane and the binding site nearest the membrane in the basic reservoir, x, is always between 0 and L. The chemical state of the rotor is determined by the state of all the binding sites in the acidic reservoir. In general, if there are N binding sites on this side, the total number of chemical states is 2^N. However, for now we focus on the binding site nearest the membrane. In this case there are just two states: "off" if this site is unprotonated and "on" if it is protonated. In the previous chapter, the mechanochemistry of the motor was described by the following set of coupled diffusion equations:

$$\frac{\partial p_d}{\partial t} = D\frac{\partial}{\partial x}\left(\frac{F_L - F_I}{k_B T}p_d + \frac{\partial p_d}{\partial x}\right) - \bar{k}_p p_d + k_d p_p, \tag{13.27}$$

$$\frac{\partial p_p}{\partial t} = D\frac{\partial}{\partial x}\left(\frac{F_L - F_I}{k_B T}p_p + \frac{\partial p_p}{\partial x}\right) + \bar{k}_p p_d - k_d p_p, \tag{13.28}$$

where $p_p(x,t)$ and $p_d(x,t)$ [1/nm] are the probability densities for being at position x and in the protonated and deprotonated states, respectively, at time t. The proton association and dissociation rates in basic reservoir are $\bar{k}_p$ [1/sec] and k_d [1/sec], respectively. Note, that dimensions of some of the model parameters and variables are different in this limit.

We can nondimensionalize these equations using the re-scaled coordinate, $(x/L) \to x$, the re-scaled time, $k_d t \to t$, and the dimensionless parameters $\Lambda = (D/k_d L^2)$, $w = (F_I - F_L)L/k_B T$, and $\kappa = k_p/k_d$. The nondimensional equations have the form:

$$\frac{\partial p_d}{\partial t} = \Lambda\frac{\partial}{\partial x}\left(w p_d + \frac{\partial p_d}{\partial x}\right) - \kappa p_d + p_p, \tag{13.29}$$

$$\frac{\partial p_p}{\partial t} = \Lambda\frac{\partial}{\partial x}\left(w p_p + \frac{\partial p_p}{\partial x}\right) + \kappa p_d - p_p. \tag{13.30}$$

Equations (13.29) and (13.30) are second order partial differential equations. This means that four boundary conditions are required in order to have a mathematically complete description of the problem. One boundary condition is that $x = 0$ is reflecting:

$$\left[w p_d + \frac{\partial p_d}{\partial x}\right]_{x=0} = 0, \tag{13.31}$$

This takes into account the fact that an unprotonated site cannot pass back through the membrane. The remaining three boundary condtions requires knowing the state of all the binding sites in the basic reservoir, which would necessitate solving a large number of coupled diffusion equations (one for each possible chemical state of the rotor). However, to keep things simple, we construct a reflecting boundary condition at $x = 1$ (x is now measured in units of L) when the rotor is in the protonated state. That is,

$$\left[w p_p + \frac{\partial p_p}{\partial x}\right]_{x=1} = 0. \tag{13.32}$$

If the proton dissociation rate is fast and the proton concentration is low in the basic reservoir. we don't expect this artificial boundary condition to have much of an effect

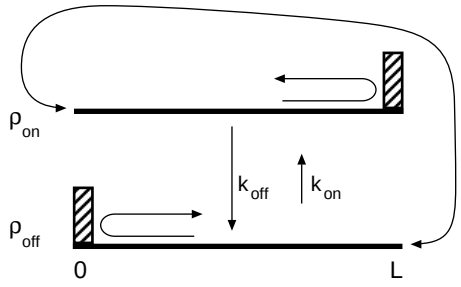

Figure 13.7 In general the chemical state of the motor is determined by all the binding sites in the right chamber. In the simplified version of the model only the binding site nearest the membrane is considered. The reflecting boundary condition in the off-state at $x = 0$ is due to the fact that an unprotonated site can not pass back through the membrane. The reflecting boundary condition in the on-state at $x = L$ is artificial and is used to simplify the problem.

since, in this limit, the probability of the first site being occupied when $x = 1$ is very small, so that this boundary condition is rarely encountered.

When an unprotonated site moves to the right of $x = 1$, it brings a protonated site out of the membrane channel and into the region $0 < x < 1$. This protonated site becomes the new site that we follow. The state of the motor goes from unprotonated to protonated, and the coordinate of the motor goes from $x = 1$ to $x = 0$. Conversely, when a protonated site moves into the membrane, it brings an unprotonated site into the region $0 < x < 1$. This unprotonated site becomes the new site we follow. The state and the coordinate of the motor change accordingly. These considerations are illustrated in Fig. 13.7 by the arrows connecting the right end of p_d to the left end of p_p. The boundary conditions that model this situation are:

$$\left(wp_d + \frac{\partial p_d}{\partial x}\right)_{x=1} = \left(wp_p + \frac{\partial p_p}{\partial x}\right)_{x=0}, \quad p_d(1,t) = p_p(0,t), \tag{13.33}$$

which is the mathematical statement of the fact that the rotor in the off-state at $x = 1$ is equivalent to the rotor in the on-state at $x = 0$. Therefore, to implement these boundary conditions numerically, we make use of the periodic boundary condition discussed in the previous chapter. Note that there are two mechanisms for changing the chemical state of the rotor: movement of the rotor and chemical kinetics.

We are now in a position to use the numerical algorithm to approximate Equations (13.29 - 13.33). The interval $(0, 1)$ is divided into M segments. For each of the M grid points, there are two possible states of the rotor, off- and on-states. Therefore, there are $2M$ possible states in the discrete approximation of the process. Let the first M states correspond to the off-state, and the states $M + 1$ to $2M$ correspond to the on-state. The equations used in the numerical scheme for $1 < n < M$ are:

$$\begin{aligned}
\frac{dp_n}{dt} &= (F_{n-1/2}p_{n-1} - B_{n-1/2}p_n) - (F_{n+1/2}p_n - B_{n+1/2}p_{n+1}) - \kappa p_n + p_{n+M}, \\
\frac{dp_{n+M}}{dt} &= (F_{n-1/2}p_{n-1+M} - B_{n-1/2}p_{n+M}) - (F_{n+1/2}p_{n+M} - B_{n+1/2}p_{n+1+M}) - p_{n+M} + \kappa p_n,
\end{aligned} \tag{13.34}$$

and the equations used to implement the boundary conditions are:

$$\frac{dp_1}{dt} = -(F_{3/2}p_1 - B_{3/2}p_2) - \kappa p_1 + p_{M+1}, \tag{13.35}$$

$$\frac{dp_M}{dt} = (F_{M-1/2}p_{M-1} - B_{M-1/2}p_M) - (F_{1/2}p_M - B_{1/2}p_{M+1}) - \kappa p_M + p_{2M}, \tag{13.36}$$

$$\frac{dp_{M+1}}{dt} = (F_{1/2}p_M - B_{1/2}p_{M+1}) - (F_{3/2}p_{M+1} - B_{3/2}p_{M+2}) - p_{M+1} + \kappa p_1, \tag{13.37}$$

$$\frac{dp_{2M}}{dt} = (F_{M-1/2}p_{2M-1} - B_{M-1/2}p_{2M}) - p_{2M} + \kappa p_M. \tag{13.38}$$

The potential used in the F_n and B_n is $\phi(x) = (F_L - F_I)x$. Note that because of the chemical kinetics, the matrices $\mathbf{A}$ and $\mathbf{C}$ required for the numerical scheme, are no longer tridiagonal. However, they are still sparse, so that solving (12.59) is not computationally expensive.

Let us discuss briefly how to calculate the protonation and deprotonation rates, $\bar{k}_p$ and k_d. The chemical reaction is:

$$\text{site}^- + \text{H}^+ \leftrightarrow \text{site} \cdot \text{H}. \tag{13.39}$$

At equilibrium, protonation and deprotonation balance. That is,

$$\bar{k}_p[\text{site}^-] = k_d[\text{site} \cdot \text{H}]. \tag{13.40}$$

Proton concentrations are generally reported as a pH value:

$$\text{pH} = -\log_{10}[\text{H}^+], \quad [\text{H}^+] = 10^{-\text{pH}}. \tag{13.41}$$

The higher the pH value, the lower the proton concentration. The pK_a value of the binding site is calculated from the measured concentration values of $[\text{site}\cdot\text{H}]$ and $[\text{site}^-]$ as:

$$\text{pK}_a = \text{pH} + \log_{10}\frac{[\text{site} \cdot \text{H}]}{[\text{site}^-]}. \tag{13.42}$$

Combining (13.40) and (13.42), we see that the rates $\bar{k}_p$ and k_d are related to pH and pK_a by

$$\frac{\bar{k}_p}{k_d} = 10^{\text{pK}_a - \text{pH}}. \tag{13.43}$$

Generally, $\bar{k}_p$ is limited by the rate at which protons diffuse to the binding site. In this limit, the association rate can be computed from the Smoluchowski formula (this rate is proportional to the proton concentration, c^{base}):

$$\bar{k}_p = \begin{pmatrix} \text{proton} \\ \text{concentration} \end{pmatrix} \cdot \begin{pmatrix} \text{absorption rate to a perfectly} \\ \text{absorbing disk of radius } r \end{pmatrix}$$

$$= \underbrace{0.6\text{nm}^{-3} \cdot 10^{-\text{pH}}}_{\text{protons/nm}^3} \cdot \underbrace{4\, r\, D_{proton}}_{\text{absorption rate}} \quad . \tag{13.44}$$

Here D_{proton} is the diffusion coefficient of protons. If we know $\bar{k}_p$, k_d can be determined by (13.43). The table shown below lists typical parameter values for ATP synthase.

Parameter Name	**Parameter Value**
Diffusion coefficient of the rod	$D = 10^4 \text{nm}^2/s$
pK_a value of binding site	$\text{pK}_a = 6.0$
pH of the right compartment	pH = 6.0 to 8.0 (variable)
External load force on the rod	$F_L = 0$ to 3 pN (variable)
Distance between binding sites	$L = 8$ nm
Diffusion coefficient of proton	$D_{proton} = 10^{10} \text{nm}^2/s$
Absorbing radius of binding site	$r = 0.5$nm

Note, that at these values of the model parameters, at pH = 7, the values of the nondimensional parameters are: $\Lambda \simeq 0.1, \kappa \simeq 0.1, w \sim 1$.

We now have all the necessary information to use the numerical scheme. Fig. 13.8A shows the relaxation of the marginal density $p(x,t) = p_p(x,t) + p_d(x,t)$ to steady state. The (dimensional) average velocity is a steady-state property of the system and is related to the total flux by the relations:

$$\langle V \rangle = LJ = -LD \left[(\frac{F_L - F_I}{k_B T} \left(p_p^{(s)} + p_d^{(s)} \right) + \frac{\partial}{\partial x} \left(p_p^{(s)} + p_d^{(s)} \right) \right], \tag{13.45}$$

where the superscript s in the above equation stands for steady state. Once steady-state is achieved, the average velocity $\langle V \rangle$ can then be computed from the relation:

$$\langle V \rangle = L(F_{n-1/2} p_{n-1} - B_{n-1/2} p_n) + L(F_{n-1/2} p_{n-1+M} - B_{n-1/2} p_{n+M}) \tag{13.46}$$

for $1 < n < M$. Typical results for the mean velocity are shown in Fig. 13.8B and Fig. 13.8C.

13.5 Other motor proteins

As we discussed in Chapter 12, there is such a variety of protein motors that no classification scheme can do justice to their diversity. However, for the purposes of discussion we can identify several physical properties that delineate classes of motors. The literature on molecular motors is vast, so we shall restrict our discussion here to those for which reasonably complete mathematical models exist as outlined in Table 13.5. Some of the most important characteristics of molecular motors are:

Fuel. The two most common energy sources for molecular motors are nucleotide hydrolysis (e.g. ATP, GTP) and transmembrane ion gradients. Certain specialized motors depend on stored elastic energy that has been captured during the assembly of the motor (e.g. spasmoneme and the acrosome of *Limulus* [Mahadevan and Matsudaira, 2000]).

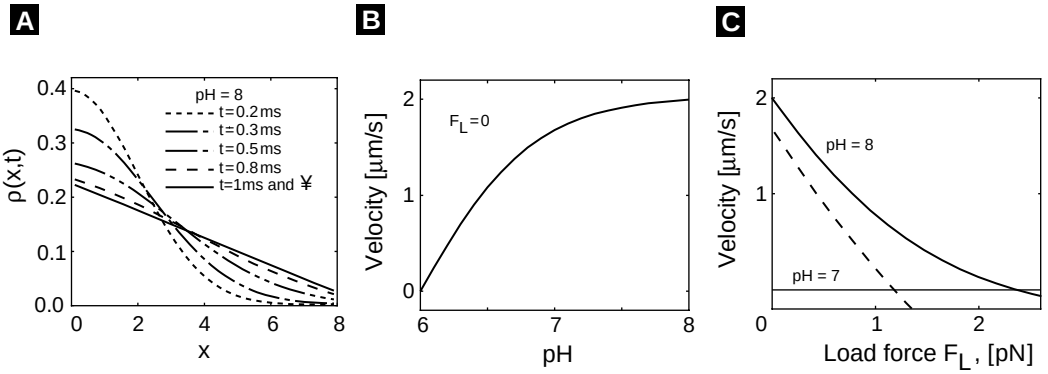

Figure 13.8 Numerical results of the simplified F_o motor. Here pH is the pH value of the right compartment. The external load force is F_L. In all the figures the number of grid points used in the simulations was $M = 32$. (A) Relaxation of the marginal density $\rho = \rho_{\text{on}} + \rho_{\text{off}}$ to steady state for pH = 8 and no external load. (B) Motor velocity as a function of pH with no external load. (C) Motor velocity as a function of the load force for pH = 7 and pH = 8.

Mechanical escapement. Three common motor types are (i) rotary (e.g. the bacterial flagellar motor, F_o ATPase); (ii) linear motors that run along a "track," usually actin, microtubules, or nucleic acid polymers (e.g. myosin, kinesin, dynein, RNA polymerase); (iii) polymerization or depolymerization motors that directly push or pull against a load (e.g. the acrosome, cellular lamellipodia, the propulsive tail of *Listeria*). The latter category suggests a subclassification into those that operate in a continuous cycle (e.g. myosin, F_1), and motors that are "one-shot" processes; i.e. they function for but a single episode of polymerization after which they are usually disassembled.

Cooperative vs "loners". Because of its small "duty cycle" (i.e. attachment time to the load), myosin II must act in concert with many other partners to produce a continuous force on an actin filament. Myosin V and kinesin, however, have longer duty cycles, and so they can transport a vesicle without the cooperation of other motors.

These categories do not begin to delineate the variety of possibilities. However, one common event generally commences the transduction process between chemical energy and mechanical force. Because molecular motors can be viewed as enzymes, the binding of a substrate onto the motor initiates the transduction process. However, this does not really tell us much, since it is simply a restatement that chemical reactions (other than isomerizations) begin by combining substrates. The feature that distinguishes molecular motors from other enzyme reactions is that the binding event is directly or indirectly coupled to the creation of mechanical forces. For example, in F_1 ATPase, the binding of ATP to the catalytic site directly generates the power stroke. However, the coupling may not always be so direct. For example, binding of a proton to the F_o rotor site switches off the local electrostatic field surrounding the rotor permitting bi-directional diffusion. The binding of monomers to polymerizing actin captures thermal fluctuations in elastic strain, which is subsequently released to power protrusion.

Several points are important. First, the role of thermal fluctuations in all these processes is central, so that none could operate when $k_B T = 0$. Second, energy captured by binding or dissociation events can be stored and released later, and in a different location, to produce mechanical work. Third, the operation of every molecular motor depends on its specialized protein geometry, so that models of motors that ignore geometry are generally not useful to biologists.

Finally, we do not believe that the operation of molecular motors involves any novel physics or chemistry. However, the amazing variety of protein shapes requires that we treat each motor individually. General principles are not likely to provide more than philosophical comfort in understanding any particular motor. In the words of Katchalsky:

"It is easier to make a theory of everything, than a theory of something"

–Aharon Katchalsky

Some molecular motors that have been modeled mathematically.

Motor	References
Acrosome	[Mahadevan and Matsudaira, 2000, Oster et al., 1982]
F_1 ATPase	[Oster and Wang, 2000, Wang and Oster, 1998, Oosawa and Hayashi, 1986]
F_o ATPase	[Elston et al., 1998, Dimroth et al., 1999, Lauger, 1991, Stein and Lauger, 1990]
Bacterial flagellar motor	[Elston and Oster, 1997, Lauger, 1990, Berry, 1993]
HSP70	[Peskin et al., 1993, Simon et al., 1992, Elston, 2000, Chauwin et al., 1998]
Kinesin	[Peskin and Oster, 1995, Fox and Choi, 2000, Derenyi and Vicsek, 1996, Keller and Bustamante, 2000]
Myosin	[Huxley and Simmons, 1971, Huxley, 1957, McMahon, 1984, Smith and Geeves, 1995]
Polymerization	[Peskin et al., 1993, Mogilner and Oster, 1996, Mogilner and Oster, 1999]
RNA polymerase	[Wang et al., 1998, Julicher and Bruinsma, 1998]

Suggestions for further reading

- *Millennial musings on molecular motors*, R. Vale. [Vale, 2000]
- *The mechanochemistry of molecular motors*, D. Keller and C. Bustamante. [Keller and Bustamante, 2000]
- *Mechanics of Motor Proteins and the Cytoskeleton*, Jonathon Howard. [Howard, 2001]

Alex Mogilner, Tim Elston, Hongyun Wang and George Oster

Exercises

1. In the example of switching in the bacterial flagellar motor, the first passage time density was calculated for the case $\Delta G = 0$. Write a program that numerically generates the first passage time density for the case when $\Delta G \neq 0$. Investigate how the distribution changes as a function of CheY concentration. Do you expect the Kramer's approximation for the mean first passage time to be valid for all values of CheY concentration?
2. Nondimensionalize equations (13.11) using the potentials

$$V_1(x) = k_B T[cos(x/L) + 0.3sin(2x/L)], \quad V_2 = 0.$$

   Use the parameters $L = 10$ nm, $D = 10^5$ nm^2/sec, 10^2 sec$^{-1} < k < 10^4$ sec^{-1}. Write a program that solves equations (13.11) numerically and compute the velocity of the flashing ratchet for various values of k from the given range. Discuss the results.

3. Simulate two rigid filaments growing side by side against a "wall," which diffuses with the diffusion coefficient D. Assume that the rates of assembly and disassembly of the monomers onto the polymer tips are known. Use the computer to model this two-filament polymerization ratchet. Estimate the rate of growth in the absence of the load force and compare it with the average velocity of the one-filament polymerization ratchet. Compare the corresponding stall forces. Do the results depend on the mutual position of two filaments?
4. Consider the following model of a "walking" molecular motor that is roughly similar to kinesin. The motor walks a 1-D track with equidistant binding sites. The motor has two "legs" that either can be (i) attached to the adjacent binding sites, or (ii) one foot is attached, while the other diffuses freely between the binding sites adjacent to the attached foot. The rate of dissociation of the front foot from the track is different from that of the rear foot. Similarly, the rate of association of the diffusing foot to the site in front of the bound foot is different from the rate of association behind the bound foot. Describe this model with coupled Smoluchowski equations and demonstrate that it is mathematically equivalent to the model considered in Section 4.1.
5. Derive Langevin equations describing the model of the "walking" motor in the previous exercise. Simulate the motor's walk numerically. By changing the association/dissociation rates find conditions under which the motor would move on average to the right. Apply a load force to the free foot directed to the left and estimate the stall force numerically.
6. Estimate numerically the average velocity and effective diffusion coefficient of the walking motor at various values of the load force. Discuss the results.

7. Assume the mechanochemical cycle of the "walking" motor is such that only the rear foot dissociates from the track, and that the diffusing foot binds only to the site in front of the attached foot (i.e. the motor makes only forward steps). Describe how to find the ratio of the association and dissociation rates if you know from an experiment the average velocity and rate of growth of the displacement variance.